PCCP

# Controlling the Self-Assembly of Perfluorinated Surfactants in Aqueous Environments



| | |
|---|---|
| Journal: | *Physical Chemistry Chemical Physics* |
| Manuscript ID | CP-ART-01-2021-000049.R1 |
| Article Type: | Paper |
| Date Submitted by the Author: | 24-Mar-2021 |
| Complete List of Authors: | Dong, Dengpan; University of Utah, Materials Science & Engineering<br>Kancharla, Samhitha; University at Buffalo - The State University of New York, Dept of Chemical & Biological Engineering<br>Hooper, Justin; University of Utah, Materials Science & Engineering<br>Tsianou, Marina; Univeristy at Buffalo, the State University of New York, Department of Chemical and Biological Engineering<br>Bedrov, Dmitry ; University of Utah, Materials Science & Engineering<br>Alexandridis, Paschalis; University at Buffalo - The State University of New York, Dept of Chemical & Biological Engineering |
| | |



SCHOLARONE™
Manuscripts

# Controlling the Self-Assembly of Perfluorinated Surfactants in Aqueous Environments

*Dengpan Dong,¶† Samhitha Kancharla,¶‡ Justin Hooper,† Marina Tsianou,‡*

*Dmitry Bedrov,†* Paschalis Alexandridis,‡**

† Department of Materials Science and Engineering, University of Utah, 122 South Central Campus Drive, Room 304, Salt Lake City, UT 84112

‡ Department of Chemical and Biological Engineering, University at Buffalo, The State University of New York (SUNY), Buffalo, NY 14260-4200

¶: Joint first authors

**Corresponding Authors**

* Paschalis Alexandridis: palexand@buffalo.edu

* Dmitry Bedrov: d.bedrov@utah.edu

ABSTRACT

Surface active per- and polyfluoroalkyl substances (PFAS) released in the environment generate great concern in the US and worldwide. The sequestration of PFAS amphiphiles from aqueous media can be limited by their strong tendency to form micelles that plug the pores in the adsorbent material, rendering most of the active surface inaccessible. A joint experimental and simulation approach has been used to investigate the structure of perfluorooctanoate ammonium (PFOA) micelles in aqueous solutions, focusing on the understanding of ethanol addition on PFOA micelle formation and structure. Structurally compact and slightly ellipsoidal in shape, PFOA micelles in pure water become more diffuse with increasing ethanol content, and break into smaller PFOA clusters in aqueous solutions with high ethanol concentration. A transition from a co-surfactant to a co-solvent behavior with the increase of ethanol concentration has been observed by both experiments and simulations, while the latter also provide insight on how to achieve co-solvent conditions with other additives. An improved understanding of how to modulate PFAS surfactant self-assembly in water can inform the fate and transport of PFAS in the environment and the PFAS sequestration from aqueous media.

***KEYWORDS*** *Perfluorooctanoate, perfluorocarboxylate, self-assembly, micelle, co-solvent effect, water*

## Introduction

Perfluoroalkyl acids (PFAAs) have been widely utilized since the 1950s as surfactants in industry, owing to their higher efficiency in reducing surface tension than their alkyl counterparts, their high thermal and chemical stability, and their immiscibility in hydrocarbons.[1,2] Fluorinated surfactants typically exhibit stronger hydrophobicity and lower critical micelle concentration (CMC) compared to their hydrocarbon counterparts.[3,4] However, the extremely low degradation rate of PFAAs in natural environments has generated widespread concerns about the contamination of water, soil, and biota.[5] Perfluorooctanoic ammonium (PFOA), typical left-over after being utilized in the emulsion polymerization of polytetrafluoroethylene or as suppressant of fires (key ingredient in aqueous film-forming foam (AFFF) fire-fighting agents), has been one of the most severe threats to drinking water at several locations in the United States and around the world,[6–10] resulting in EPA establishing the advisory level for drinking water to be 70 ng/L.[11,12] The removal of PFOA with traditional techniques, e.g., adsorption on activated carbon (AC), is substantially less efficient than non-traditional yet more expensive methods, including β-cyclodextrin-based polymer networks and porous covalent organic frameworks.[13,14,15] The sequestration from aqueous media of fluorinated surfactants can be affected by their tendency to form hemi-micelles or micelles on the surfaces of adsorbent materials.[16,17] While surface self-assembly could enhance the adsorption capacity, on many occasions it plugs the inner pores in the adsorbent material, rendering most of the active surface inaccessible.[16]

The urgency for the efficient removal of PFOA from contaminated water motivates our research on controlling the formation and morphology of PFOA micelles. Despite a few available experimental and theoretical studies focusing on PFAA self-assembly in water,[18–21] the

mechanism of PFOA micelle assembly in aqueous solutions and the effect of addition of other solvents remain poorly understood. Molecular simulations have made good progress in establishing reliable force fields for the description of fluorinated compounds,[22,23] however, we are aware of only two modeling studies on the behavior of PFAAs in aqueous environments.[24,25]

Additives such as alcohols can act as either co-solvent or co-surfactant, depending on their concentration in the aqueous surfactant solution.[26–29] Co-solvents affect the surfactant micellization indirectly by modifying the bulk solvent properties, whereas co-surfactants adsorb at the micellar surface.[26] The effects of alcohols on the surfactant micelle structure depend highly on the concentration and the alkyl chain length of the alcohol.[30–36] While substantial literature is available on the effect of ethanol on hydrocarbon surfactant micelle formation and structure, [32–39] the effect of alcohol on the self-assembly of fluorinated surfactants is less known. Thermodynamic information indicates that medium-chain alcohols can solubilize inside fluorinated surfactant micelles,[40–43] however, no information is published on the effects of short-chain alcohols (methanol, ethanol) on the micellization of fluorinated surfactants and the micelle size and structure. Quantitative correlations between the nature of the co-solvent and the micelle morphology remain unavailable.

In this we work we focus on understanding how alcohol molecules affect PFOA micelles in water via a joint and complementary experimental and simulation approach. The effect of ethanol on the self-assembly of PFOA is assessed from the critical micelle concentration (CMC) and the degree of counterion dissociation determined from conductivity measurements. The micellar microenvironment, indicative of possible ethanol solubilization in micelles, is probed by pyrene fluorescence. Small-angle neutron scattering (SANS) is employed to determine PFOA micelle size and structural changes induced by ethanol addition. The experimental measurements

are complemented by extensive atomistic MD simulations to provide molecular scale insight into the PFOA self-assembly as a function of surfactant and additive concentration.

## Materials and Methods

*Systems*: Perfluoro-n-octanoic acid ammonium salt ($C_7F_{15}COONH_4$, CAS number: 3825-26-1, MW = 431.1 g/mol, 98% purity), also known as ammonium perfluorooctanoate (PFOA), was obtained from SynQuest Laboratories (Alachua, FL, USA) and used as received. Ethanol ($CH_3CH_2OH$), 200 proof, ACS/USP grade was obtained from Pharmco (Brookfield, CT, USA). Deuterium oxide (99.9% D), ($D_2O$, MW = 20.03 g/mol, 99.5% purity), also known as deuterated water, and ethanol-D6 (99% D), ($CD_3CD_2OD$, MW = 52.11 g/mol, 99.5% purity), also known as deuterated ethanol, were obtained from Cambridge Isotope Laboratories, Inc. (Tewksbury, MA, USA) and used as received. Samples used in small-angle neutron scattering (SANS) were prepared using $D_2O$ and D-ethanol. Samples used in conductivity, surface tension, and pyrene fluorescence were prepared using milli-Q purified water (0.055 μS/cm) and H-ethanol. Throughout this study, 10% and 20% ethanol refer to 10 wt% and 20 wt% of ethanol relative to plain water.

*Conductivity:* Accumet XL 50 and Model 20 conductivity meters (Fisher Scientific, Hampton, NH, USA) with potassium chloride electrodes were used to measure conductivity. Temperature corrections were taken into account while standardizing the conductivity meter for more accurate readings. Conductivity in aqueous solution in the absence and in the presence of ethanol was measured at 23 °C (±1 °C) in the PFOA concentration range 0 – 50 mM. The break point and the slopes of conductivity vs surfactant concentration curve can be used to determine the critical micellization concentration (CMC) and the degree of counterion dissociation.[44] The

ratio of the conductivity vs. surfactant concentration slopes above ($S_2$) and below ($S_1$) the CMC gives the degree of counterion dissociation ($\alpha = S_2/S_1$).[27]

*Micropolarity:* Pyrene fluorescence spectroscopy was used to study the micropolarity of aqueous surfactant solutions. 2 μL of 1 mM pyrene (Fluka, Buchs, Switzerland) in ethanol was added to 3 g sample solutions. The resulting overall pyrene and ethanol concentrations were about 0.7 μM and 6.7 x 10-4 vol %, respectively. Pyrene fluorescence spectra of PFOA aqueous solution in the absence and in the presence of ethanol were recorded at 22 °C for PFOA concentration 0.1–200 mM using a Hitachi F-2500 fluorescence spectrophotometer (Stoughton, MA, USA) for 350 – 460 nm emission wavelength. The excitation wavelength of pyrene was $\lambda$ = 335 nm. The pyrene monomer emission spectrum exhibits a vibronic fine structure, and the ratio of the intensities of first and third vibronic peaks (I1/I3) strongly depends on the polarity of its microenvironment. [29,45,46] Pyrene is hydrophobic and it tends to move from the aqueous phase to a hydrophobic environment. Below CMC, the pyrene molecules are in the aqueous polar environment, and hence the I1/I3 values will be almost equal to those in the solvent (in the absence of added surfactant). Above the CMC, pyrene molecules tend to move into more hydrophobic micellar environment, which is reflected in a decrease in I1/I3 values.

*Surface tension:* When surfactant is added to an aqueous solution, the surfactant molecules accumulate at air water interface and decrease the surface tension. The surface tension of aqueous surfactant solutions was measured at 24 °C by the Wilhelmy plate method using a Kruss model K100 tensiometer. When the surface tension is plotted as a function of surfactant concentration, the surfactant concentration where surface tension reaches a plateau like region is considered as CMC. The slope of the surface tension vs logarithm of surfactant concentration plot ($d\gamma/d\log C$) determined at the CMC can be used to estimate surface properties like the

maximum surface excess concentration $\Gamma_{max}$ and the minimum area occupied by a surfactant molecule ($A_{min}$) at air/liquid interface.[47,48,49] $\Gamma_{max}$ and $A_{min}$ are given by:

$$\Gamma_{max} = -\frac{1}{2.303nRT}\left(\frac{d\gamma}{dlogC}\right)_{T,P} \quad (1)$$

$$A_{min} = \frac{1}{N\Gamma_{max}} \quad (2)$$

where $\gamma$ is the surface tension, $R$ is the universal gas constant (8.314 J mol$^{-1}$ K$^{-1}$), $T$ is absolute temperature, $C$ is surfactant concentration in mM, and $N$ is the Avogadro number.[47,49] The constant $n$ is taken as 2 for surfactants in which the surfactant ion and counterion ae monovalent.[47]

*SANS data collection and reduction:* SANS measurements of aqueous surfactant solutions in the absence and in the presence of various additives were performed on the NG-B 30 m SANS instrument at the Center for Neutron Research (NCNR), National Institute of Standards and Technology (NIST), Gaithersburg, MD. Neutrons with 6 Å wavelength were focused on samples kept in quartz cells of 2 mm or 4 mm thickness. Sample-to-detector distances (SDD) of 1.33, 4 and 13.17 m were used for each sample in order to cover the wave vector (q) range 0.05 Å$^{-1}$ < q < 0.5 Å$^{-1}$. The measurement time was in the range 180 – 4200 seconds. The raw SANS intensity data were corrected and reduced using IGOR Pro. Reduced SANS data of a particular sample at three instrument configurations (1.33, 4 and 13.17 m SDD) were combined into one data file after trimming data points from the ends of each set and rescaling the overlap regions.[50]

In the data reduction process, scattering intensity raw data were corrected for the scattering from empty cell, background and detector sensitivity, and converted to absolute intensity scale.[9] The scattering contribution from the solvent has been accounted for by fitting a straight line to the solvent intensity data in the high-q range (to avoid noisy data), and subtracting the intensity of this straight line from the sample scattering intensity. The fraction of the solvent

scattering intensity subtracted (scale factor *f*) is the volume fraction of solvent in the sample. The error bars shown in the SANS absolute intensity plots were calculated by the IGOR Pro software during the data reduction process. The data points in the low-q region may exhibit relatively large error bars due to scattering from possible tiny air bubbles present in the sample.

*SANS analysis:* SANS data from PFOA micelles in $D_2O$ in the absence and in the presence of d-ethanol have been fitted with the core-shell ellipsoid form factor and the Hayter – Penfold structure factor with rescaled mean spherical approximation (RMSA).[36]

The overall scattering intensity $I(q)$ is given by:

$$I_{micelle}(q) = A\phi P(q)S(q) + B_{inc} \quad (3)$$

$P(q)$ is the form factor representing the shape and structure of a micelle, and $S(q)$ is the structure factor representing the intermicelle interactions. $\varphi$ is the volume fraction of the micelles which in turn depends on the overall surfactant concentration. The parameters $A$ and $B_{inc}$ account for additional contributions due to the absolute scaling and incoherent noise, respectively.

The $P(q)$ was calculated using the following equations:

$$P(q) = \frac{scale}{V}F^2(q,\alpha) + background \quad (4)$$

$$F(q, \alpha) = f(q,b,a, \alpha) + f(q, b + \delta, a + \delta\epsilon, \alpha) \quad (5)$$

where $b$ is the equatorial core radius perpendicular to the rotational axis of the ellipsoid, $a$ is the polar core radius along the rotational axis of the ellipsoid, $\delta$ is the thickness of the shell near equator, $\epsilon$ is the ratio of shell thickness at pole to that at equator. For a fixed shell thickness $\epsilon = 1$.

$$F(q, R_e, R_p, \alpha) = \frac{3\Delta\rho V(\sin[qr(R_e, R_p, \alpha)] - \cos[qr(R_e, R_p, \alpha)])}{[qr(R_e, R_p, \alpha)]^3} \quad (6)$$

$$r(R_e, R_p, \alpha) = [R_e^2 sin^2\alpha + R_p^2 cos^2\alpha]^{1/2} \quad (7)$$

$\alpha$ is the angle between the axis of the ellipsoid and $\vec{q}$, $V = (4/3)\pi R_p R_e^2$ is the volume of the ellipsoid, $R_p$ is the polar radius along the rotational axis of the ellipsoid, $R_e$ is the equatorial radius perpendicular to the rotational axis of the ellipsoid and $\Delta\rho$ (contrast) is the scattering length density (SLD) difference, either ($\rho_{core} - \rho_{shell}$) or ($\rho_{shell} - \rho_{solvent}$). When the ratio of the polar core radius ($a$) to the equatorial core radius ($b$) ε (= $a/b$) < 1, then the core is oblate; when ε > 1 it is prolate, and ε = 1 denotes a spherical core.

The structure factor $S(q)$ was calculated using a Hayter−Penfold-type potential,[51] with mean spherical approximation and rescaling corrections for low volume fractions, given the micelle volume fraction, charge on a micelle, and ionic strength of the solution.[10] Parameters that are adjusted when fitting SANS intensity data with the above described form and structure factors include: scale, background, equatorial core radius or minor core radius ($b$), axial ratio of core (ε), shell thickness at equator ($\delta$), ratio of shell thickness at pole to that at equator (ϵ = 1, we considered uniform shell thickness), SLD shell ($\rho_{shell}$), SLD core ($\rho_{core}$), SLD solvent ($\rho_{solvent}$), micelle volume fraction ($\varphi$), charge on a micelle ($Z$), temperature, electrolyte concentration, and dielectric constant of the medium. The micelle association number ($\eta$), fractional charge on a micelle ($\alpha = Z/\eta$), and the number of ethanol molecules solubilized in a micelle ($\eta_E$) are other important parameters that are calculated from the parameters obtained from fitting SANS intensity data.

In analyzing the SANS data, we fix the known parameters (e.g., solvent SLD, temperature, ionic strength, and dielectric constant of the medium), we make assumptions for some parameters (e.g., minor core radius ($b$) is set equal to the extended length of a $PFO^-$ fluorocarbon chain, ratio of shell thickness at pole to that at equator ϵ = 1 (uniform shell thickness)), and we leave some parameters (e.g., background, volume fraction ($\varphi$), charge on a

micelle ($Z$), shell thickness at equator ($\delta$)) free to be adjusted in order to obtain a best fit value. The statistical parameter $\chi_R^2$ provided by the software quantifies the differences between the calculated and the experimental SANS intensities. $\chi_R^2$ tends to unity for a perfect fit. Details are provided in what follows.

SANS intensity data from PFOA solutions in the $q$-range 0.01 - 0.5 Å$^{-1}$ were fitted using the core-shell ellipsoid form factor and Hayter – Penfold structure factor. Table S1 presents values of molecular parameters used for SANS data fittings.

For the PFOA in $D_2O$ system we considered that the micelle core comprises of only fluorocarbon chains (dry core), and the shell comprises of carboxylate head groups, counterions, and associated water molecules. This assumption of water-free core was previously used in the SANS analysis for sodium perfluorooctanoate (NaPFO) and cesium perfluorooctanoate (CsPFO).[16,52,53] We also examined other possible cases in which 1 or 2 $CF_2$ groups of the $PFO^-$ fluorocarbon chain will be in the micelle shell in contact with water. Analysis considering some water penetration into the fluorocarbon region of the micelle was reported in a NaPFO SANS study,[16] however, this paper did not report parameters obtained from SANS analysis considering water penetration. This study stated that NaPFO micelles with fluorocarbon chains residing in water-free core (0 $CF_2$ groups in contact with water) agreed best with the SANS data.[16] An analysis of SANS data for sodium perfluorononanoate (NaPFN) micellar solutions using a form factor for spheres and Hayter-Penfold-Hansen spherical macro-ion model structure factor concluded that "although core-shell $P(Q)$ function for spheres was investigated here, there was no clear evidence in the SANS data for distinct fluorocarbon core and head group plus counterion shell regions, therefore, $P(Q)$ depends primarily on the micelle radius $r$".[54]

In the case of PFOA in $D_2O$ + 10% or 20% d-ethanol systems, we considered three scenaria for the micelle composition:

Scenario 1: The micelle core consists of the $PFO^-$ whole fluorocarbon chains and the $CD_3CD_2$ parts of the d-ethanol molecules that are solubilized in the micelles, while the micelle shell consists of the carboxylate head-groups of $PFO^-$, counterions, polar -OD groups of d-ethanol molecules solubilized in the micelles, and associated water molecules.

Scenario 2: The micelle core consists of only $PFO^-$ fluorocarbon chains, and the shell consists of the $PFO^-$ carboxylate head-groups, counterions, the whole d-ethanol molecules associated with the micelle, and associated water molecules.

Scenario 3: The micelle core consists of only $PFO^-$ fluorocarbon chains, and the shell consists of 1 or 2 $CF_2$ groups from the $PFO^-$ chains, $PFO^-$ carboxylate head-groups, counterions, d-ethanol molecules associated with the micelle, and associated water molecules (in this scenario, 1 or 2 $CF_2$ groups from $PFO^-$ will be in close contact with the ethanol molecules and with water).

Discussion of specific details for the analysis using each scenario can be found in the Supplementary Information (SI). The results from each of the three scenaria considered here support the “cosurfactant” effect at 10% ethanol and the “cosolvent” effect at 20 % ethanol. The micelle association numbers obtained from the three scenaria are almost the same. Similar number of ethanol molecules per micelle at 20% ethanol are obtained from the three scenaria. A qualitative analysis of the SANS scattering profiles suggests that micelles become smaller with increasing ethanol concentration. However, in scenario 3, the size of the micelle did not decrease for 10% ethanol. In scenario 2, we considered the complete ethanol molecules to reside in the micelle shell, however, our pyrene fluorescence results suggest ethanol solubilization in PFOA

micelles into which pyrene prefers to locate (in the palisade layer). On the basis of the above, and for consistency with the case when no ethanol is present, we report in what follows the parameters resulting from scenario 1 in describing the PFOA micelle structure in ethanol-water mixtures. The parameters obtained from scenario 2 and 3 can be found in SI.

*Simulations:* Molecular dynamics (MD) simulations were conducted employing a non-polarizable version of the Atomistic Polarizable Potentials for Liquids, Electrolytes and Polymers (APPLE&P) force field.[55,56] Due to the very low CMC values of PFOA in water, simulations were conducted at surfactant concentrations higher than the reported CMC at 298 K. A typical system contained 32 $PFO^-$ chains, 32 $NH_4^+$ counterions and about 4032 water (or water + co-solvent) molecules, which corresponds to 390mM PFOA concentration. Such setup is sufficient to observe the formation of one PFOA micelle in pure water, and enables the investigation of the influence of additives on the micelle structure. Additional MD simulations with a scaled dipole moment of the O-H bond in the ethanol molecules were also conducted in order to capture the diversity in the choice of additives. Molecules with high dipole moments effectively represent additives that are more hydrophilic, whereas molecules with noticeably reduced dipole moments emulate more hydrophobic additives. Note that the time-scales accessible for atomistic MD simulations are not sufficient to access the time-scales of micelle breaking or merging and, therefore, it is necessary to keep in mind that the obtained structural analysis can be affected by the finite system size and observation time of the MD simulations.

The molecular representation and atom labels can be seen in Figure S3. The force field parameters and functional forms are given in Table S5. All simulations were conducted at 298 K, with temperature controlled by the Nose-Hoover thermostat and barostat.[57] The cut-off radius for the van der Waals (VDW) and real part of Ewald summation[58] for electrostatic interactions was

set to 15 Å, with a tapering distance of 0.5 Å. A multiple time step integration scheme has been applied with a 0.5fs time step for all bonds and bends, a 1.5 fs time step for integration of dihedrals and short-range (less than 8.0 Å) non-bonded interactions, and a 3fs time step for the remaining non-bonded interactions and electrostatic reciprocal space portion. All bond lengths were constrained with the SHAKE algorithm using $10^{-14}$ tollerance.[59] Initially, all molecules and ions were placed randomly in a relatively large cubic simulation cell (300 Å in each dimension). Within 300 ps, the simulation cell was shrunk to the dimensions close to the equilibrium size. Subsequent equilibration simulations were conducted in the NPT ensemble in order to establish equilibrium density of the system. Production runs over 30 ns were also conducted in the NPT ensemble.

## Results and Discussion

*Self-assembly of micelles*: The CMC of PFOA in aqueous solution in the absence of ethanol is 26.5 (±0.1) mM and in the presence of 10% or 20% ethanol is 14.2 (±0.5) mM or 13 (±0.2) mM (46% or 51% decrease compared to the case with no ethanol), respectively, as indicated by conductivity experiments (

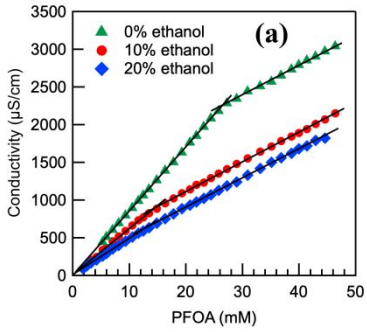

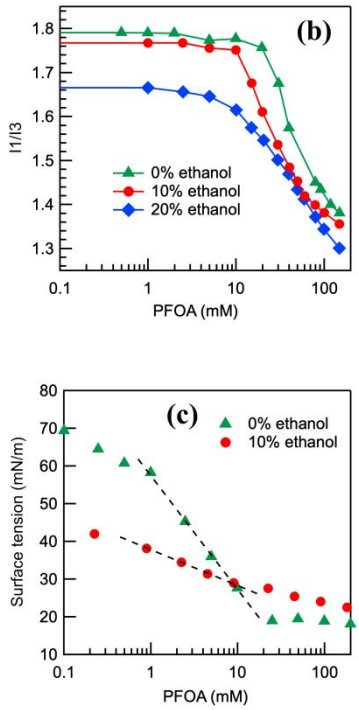


*Figure 1*a). The conductivity also provided the degree of counterion dissociation ($\alpha$) of PFOA in aqueous solution: 0.47 in the absence of ethanol, and 0.63 or 0.78 in the presence of 10% or 20% ethanol, respectively (34% or 66% increase compared to the case of zero ethanol). When 10% of ethanol is added to water, the CMC of PFOA decreased to almost half its value in pure water. However, when the ethanol concentration is further increased to 20%, only a minor additional reduction in the CMC is observed. This initial CMC decrease with ethanol concentration may be attributed to the solubilization of ethanol molecules in surfactant micelles, which decreases the surface charge density and head group-head group repulsion at the micellar surface lowering the CMC (co-surfactant effect).[19,20] However, at higher ethanol concentrations (20%), the three-dimensional water structure network is disrupted, resulting in a decrease of the hydrophobic effect and an increase in the CMC. Therefore, in the case of PFOA solution with 20% of ethanol in water, two effects modulate the self-assembly: (i) disruption of the water structure network, decreasing hydrophobic effect, and increasing CMC, and (ii) solubilization of ethanol molecules

in the PFOA micelles, reducing the surface charge density and decreasing CMC (co-solvent effect). Similar CMC variation has been observed in the case of the common surfactant sodium dodecyl sulfate (SDS).[36,37]

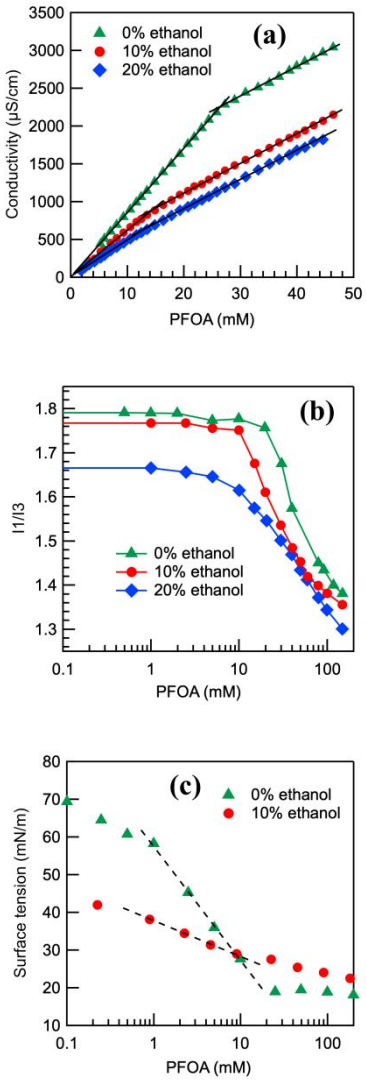


*Figure 1. (a) Conductivity of PFOA aqueous solutions in the presence of various concentrations of ethanol; (b) pyrene fluorescence intensity I1/I3 ratio of PFOA aqueous solutions in the absence and in the presence of 10 or 20 wt% ethanol (the lines are guides to the eye); (c) surface tension of PFOA aqueous solutions in the absence and in the presence of 10 wt% ethanol. The surface tension of 10% ethanol – water mixture in the absence of surfactant is 49.1 mN/m.*

The pyrene fluorescence intensity I1/I3 ratio of PFOA aqueous solutions in the absence and in the presence of added ethanol decreases due to the formation of micelles (

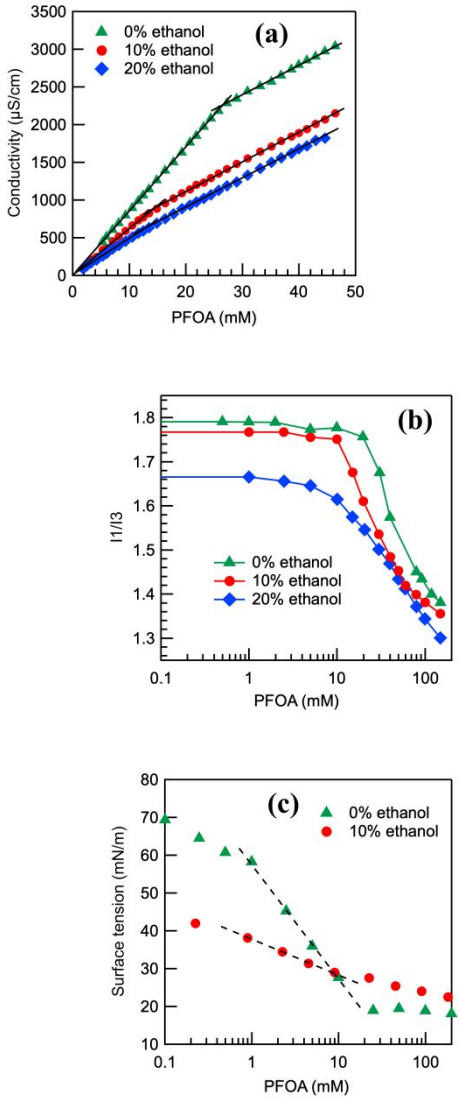


Figure 1b). Similar behavior has been observed previously with pyrene for fluorinated aqueous solutions.[60,61] This was ascribed to the pyrene molecules residing in the outer palisade layer of the surfactant micelles due to the immiscibility between pyrene and the fluorocarbon core.[45] The CMCs estimated from I1/I3 ratios are in good agreement with the

values determined based on conductivity measurements. The micro-polarity sensed by pyrene decreased with ethanol concentration (Figure S1 in the SI) possibly due to pyrene moving into the vicinity of ethanol that is solubilized in PFOA micelles (for details, please refer to SI).

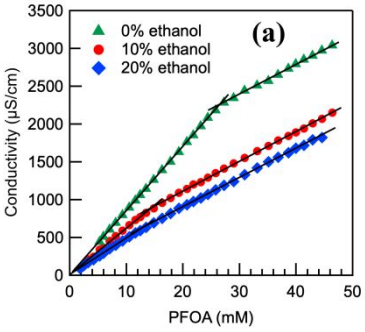


Analysis of the surface tension data (

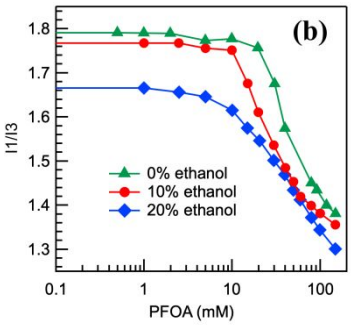


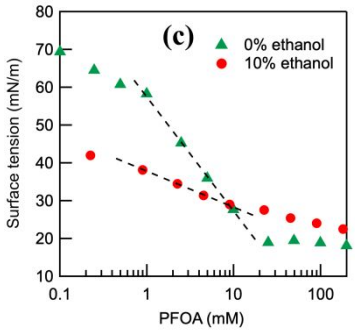


Figure 1c) indicates the surface area per PFOA head-group $A_{min}$ = 64 ± 2 Å$^2$ in plain water, while for PFOA in 10% ethanol in water mixture $A_{min}$ = 200 ± 4 Å$^2$. The greater surface area per $PFO^-$ head-group in 10% ethanol aqueous solution indicates a looser packing of PFOA at the micelle surface. The critical packing parameter (CPP) changed from 0.47 to 0.15 with 10%

ethanol addition (for details, please refer to the SI). The big increase in surface area, decrease in CPP, and changes in the micellar microenvironment sensed by pyrene with ethanol suggest the localization of ethanol at the PFOA micelle surface and interior, and possible micelle shape change. SANS experiments and molecular modelling of our PFOA system provide information regarding the effect of ethanol on the PFOA micelle structure.

*Micelle structure:* SANS intensity profiles from 110 mM PFOA in $D_2O$ and in d-ethanol $D_2O$ solutions, and the corresponding fits using the form and structure factor described above and in SI, are shown in

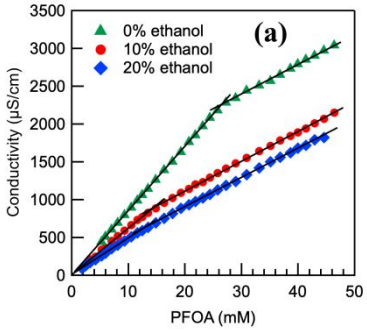


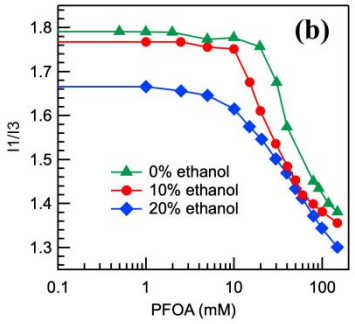


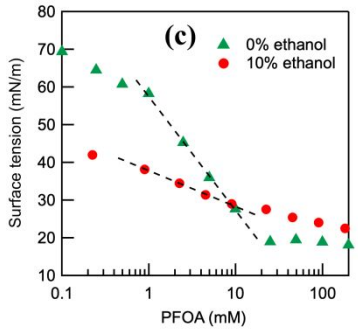

Figure 1. The pronounced correlation peak, reflecting repulsive interactions between the micelles, shifts to higher $q$ values as the ethanol concentration increases, indicating a decrease in the inter-micelle distances, $d$. Since the surfactant concentration was kept constant, such a decrease in $d$ reflects an increase in the micelle number density, which is possible only if the micelles become smaller (recall that the concentration of non-associated surfactant, i.e., CMC, decreases with added ethanol). The peak intensity decreases with the addition of ethanol, indicating weaker electrostatic repulsions between the micelles.

The influence of added ethanol on select properties of micelles can be seen in Figure 2b. The micelle association number at 110 mM PFOA aqueous solution in the absence of ethanol is 30, while in the presence of 10% or 20% d-ethanol it becomes 17 or 12, respectively (44% or 60% decrease compared to the case of zero ethanol). The fractional charge on a micelle, $\alpha$, increased by 170% and 180% upon ethanol addition at 10% and 20% levels, respectively. The average number of ethanol molecules solubilizing in a PFOA micelle is 16 at 10% ethanol and 8 at 20% ethanol. The decreased number of micelle-solubilized ethanol molecules upon increasing ethanol concentration from 10% to 20% support a "co-surfactant" effect at 10% ethanol and a "co-solvent" effect at 20 % ethanol. The volume percent of ethanol in a micelle also decreased. The volume of a micelle (including bound counterions, hydration water, and ethanol) decreased by 34% and 55% in the presence of 10% and 20% ethanol, respectively (refer to Supplementary Info, Table S2).

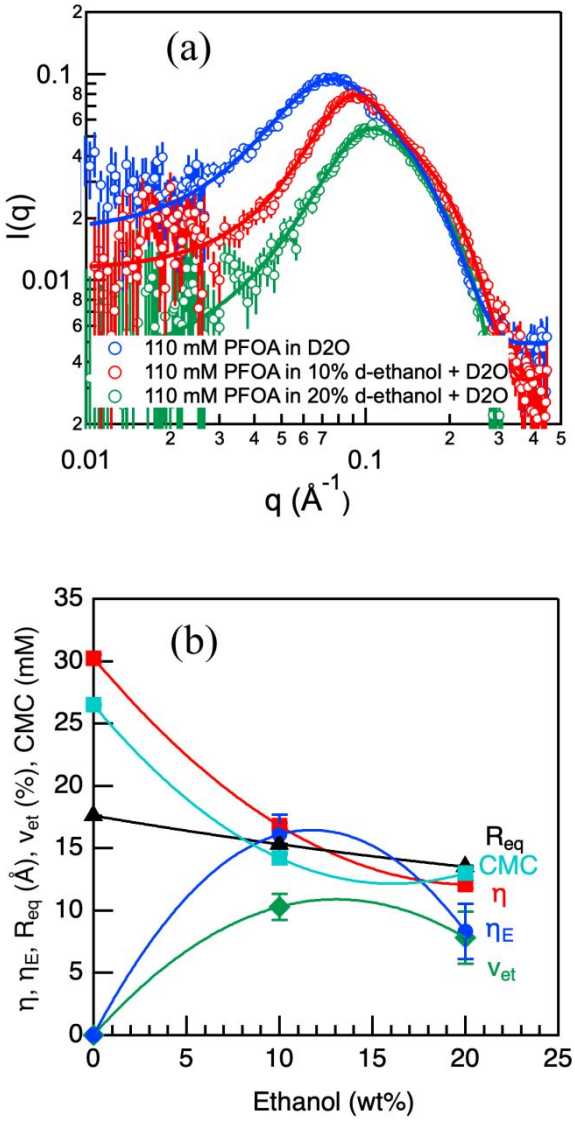


*Figure 2. (a) SANS intensity profiles of PFOA in $D_2O$ and in d-ethanol + $D_2O$ solutions, corrected for solvent scattering (markers represent intensity data points and solid lines represent the fits using models described in the text); (b) micelle association number (η), average number of ethanol molecules per micelle ($\eta_E$), radius (in Å) of a sphere with volume equal that of the micelle ($R_{eq}$), volume percent of ethanol ($v_{et}$) in a micelle which comprises [$PFO^-$ + hydration water + counterions + ethanol], and CMC (in mM), plotted as a function of ethanol content in the aqueous solution (the lines are guides to the eye).*

PFOA micelles formed in molecular dynamics (MD) simulations of systems with different concentrations of ethanol are shown in Figure 3. Owing to the strong electrostatic attraction between the anionic head-group of $PFO^-$ and the counterion, the acetate groups and

$NH_4^+$ counterions tend to form tightly packed clusters in pure water. Around 40% of $NH_4^+$ is dissociated from the surfactant and is fully solvated by water without contacting the acetate group. Figure S4 shows the average number density profiles of F atoms and COO group of $PFO^-$ as a function of distance (r) from the PFOA micelle center of mass. For the case of pure water, we can see that, when r becomes larger than 10 Å, the density of F atoms drops sharply, which is consistent with the extended length of the C8 chain that is taken in the SANS analysis as the minor radius of the micelle core. As expected, the COO head-groups are located on the surface of the micelle with the peak in density probability at $r \approx 14$ Å. Note that, despite the compact shape of the micelle in water (Figure 3a), the number of COO groups is not sufficient to cover the entire micelle surface. As a result, about 55% of F atoms are in direct contact with water. With the increase of ethanol concentration from 0 to 25 wt%, the PFOA micelles become more diffuse (Figure 3). As can be observed from Figure 3b, in which the $PFO^-$ molecules are highlighted with semitransparent yellow isosurfaces, the hydrocarbon tails of ethanol molecules show an affinity to the hydrophobic fluorocarbon chains of $PFO^-$, consistent with the Scenario #1 of SANS data analysis discussed above. At relatively low ethanol content (i.e., 5% and 13%), the ethanol molecules are located primarily at the micelle surface, retain their tight binding with water and, at the same time, eliminate unfavorable F-water contacts. This is consistent with the co-surfactant behavior of ethanol. When the ethanol concentration increases to 25%, the ethanol molecules penetrate into the interior of the micelle, as shown in Figure 3, demonstrating miscibility between ethanol and PFOA. The strong influence of 25% added ethanol on the micelle structure is consistent with the co-solvent character of ethanol.

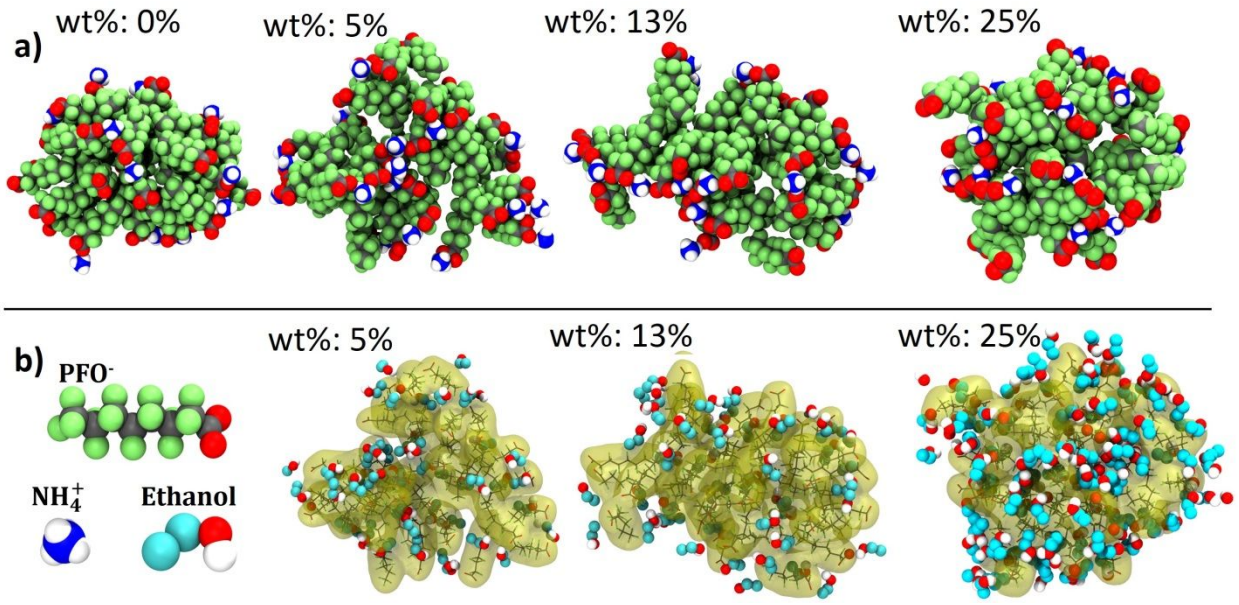


*Figure 3. (a) Morphologies of PFOA micelles at 5, 13 and 25 wt% ethanol, obtained from MD simulations; and (b) distribution of ethanol molecules near the micelle at the corresponding compositions from panel (a).*

From MD simulations, it is straightforward to calculate the radius of gyration tensor of the micelle:

$$S_{kl} = \frac{1}{M} < \sum_{i=1}^{N} m_i k_i l_i > \quad (8)$$

where $N$ is the number of $PFO^-$ atoms in the micelle (excluding ammonium counterions), $k_i$, $l_i$, are $x$, $y$, $z$ coordinates of atom $i$ relative to the position of the micelle center of mass, $m_i$ is atomic mass of atom $i$, $M$ is the total mass of atoms comprising the micelle, and < > defines averaging over the whole trajectory. Diagonalization of this matrix gives the principal moments of radius of gyration $S_{xx}$, $S_{yy}$, and $S_{zz}$ that can be used to calculate the average radius of gyration $R_g^2 = S_{xx} + S_{yy} + S_{zz}$ and assess the ellipsoidal shape of the micelle. In pure water, $R_g^2$ = 139.1 Å$^2$ with corresponding principle moments of $S_{xx}$ = 31.3 Å$^2$, $S_{yy}$ =43.5 Å$^2$, and $S_{zz}$ =62.9 Å$^2$, indicating a prolate ellipsoidal shape of the micelle where one axis is noticeably larger than the other two. The ratios of the principal moments of gyration indicate that the difference between the largest

and the smallest components is about 40% ($\sqrt{S_{zz}/S_{xx}} = 1.4$) consistent with the prolate micelle shape obtained from SANS analysis. Figure 4 shows the change of the micelle $R_g^2$ as a function of ethanol concentration (black line corresponding to $\mu/\mu_0$=1.0 case). With addition of ethanol, the micelle size expands somewhat, which is consistent with the observed interpenetration of ethanol into the micellar core and the overall loose shape of the micelle seen in Figure 3. The micelle shape asymmetry also increases with the principle moments of gyration becoming $S_{xx}$ = 32.9 Å$^2$, $S_{yy}$ =53.6 Å$^2$, and $S_{zz}$ =96.1 Å$^2$ in solution with 25% of ethanol. At this concentration, the micelle changes towards oblate shape where one dimension becomes noticeably smaller than the other two. The principal components of the gyration tensor are shown in Figure S6 as a function of ethanol concentration. Note that direct comparison of the radius of gyration between SANS and MD simulation is complicated because the MD simulations were conducted with a fixed number of $PFO^-$ molecules ($N$=32) in the micelle while, in the analysis of SANS data, the association number is an adjustable parameter. Analysis of experimental data shows that, with increase of ethanol concentration and penetration of ethanol into micelle, the association number is decreasing significantly and, hence, it is natural to expect a reduction in the micelle diameter. In simulations, the penetration of ethanol into the micelle leads to its expansion and the formation of a loose structure, which eventually (if simulations could access much longer time and length scales) would lead to the breaking into several smaller micelles. Therefore, instead of directly comparing the micelle dimensions obtained from SANS and MD simulations, it is more instructive to focus on the observed trends and the consistency of the observed phenomena.

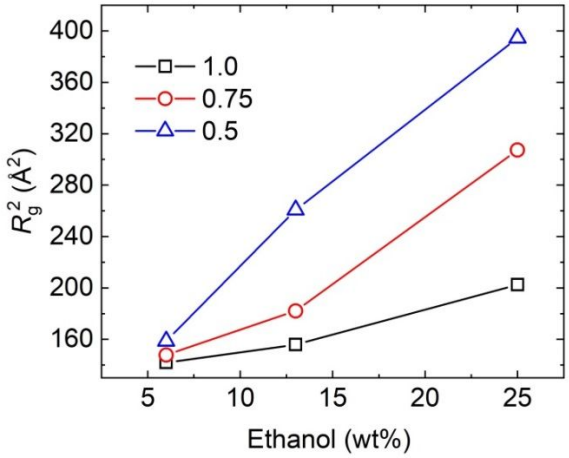


*Figure 4. Radius of gyration of PFOA micelle as a function of additive content and relative (to ethanol) molecular dipole moment ( $\mu/\mu_0$=1.0 corresponds to real ethanol molecule without dipole rescaling).*

To obtain a more complete picture of the changes in micelle structure, we also evaluated the density distribution of ethanol molecules with respect to the micelle center (as defined by $PFO^-$ molecules), which is shown in Figure 5. At low concentrations of additive (up to 13%), the additive molecules are located primarily on the micelle surface and are not able to penetrate into the interior space of the micelle (consider black lines corresponding to $\mu/\mu_0$=1.0 case). Such behavior is clearly identifying the co-surfactant role of ethanol. However, in solutions with 25% of ethanol, we can see that ethanol molecules start to penetrate inside the micelle core, indicating a transition to a co-solvent regime.

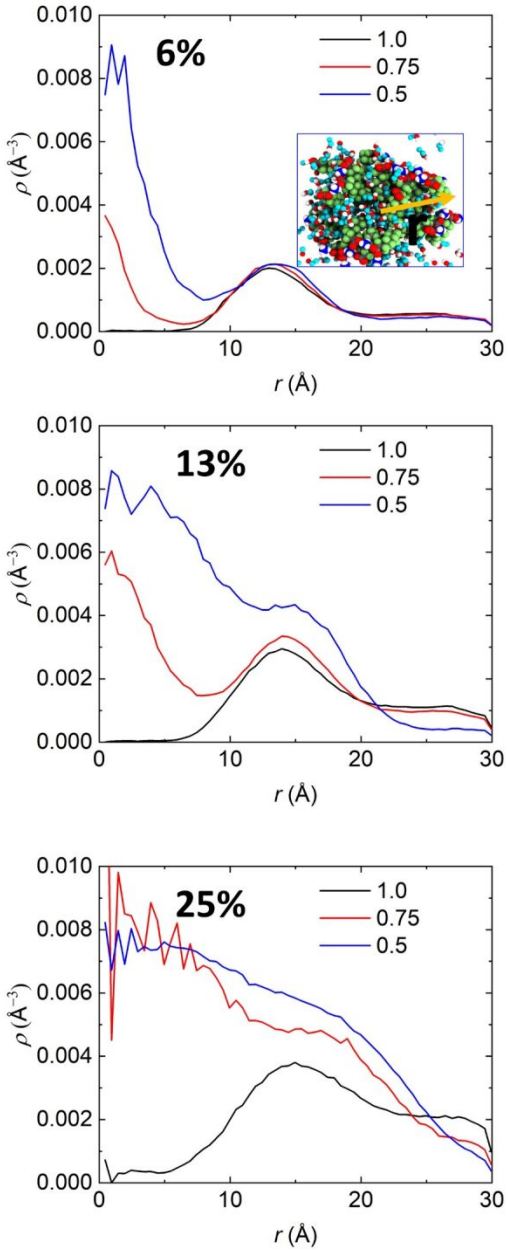


*Figure 5. Radial density profile of additive molecules from the center of PFOA micelle, for different scaling of ethanol dipole moments ($\mu/\mu_0$=1.0 corresponds to real ethanol molecule without dipole rescaling).*

*Influence of additive polarity*: To expand our understanding of how characteristics of additives can influence the transition from co-surfactant to co-solvent behavior, we have conducted MD simulations in which the dipole moment (μ) of ethanol molecules was reduced to mimic the influence of solvents with weaker binding to water; to this end, $\mu/\mu_0$ ratios have been

investigated in the 1.0-0.5 range (where $\mu_0$ = 1.765 D is the original dipole moment of ethanol). In this mixture, the hydrogen bonds between $H_2O$ and ethanol can be formed in two ways: (1) $H_{ethanol}$ as the hydrogen bond donor and $O_{H2O}$ the acceptor, and (2) $H_{H2O}$ as the hydrogen bond donor and $O_{ethanol}$ the acceptor. According to *ab initio* calculations for the $H_2O$-ethanol dimer, the second type of bonding has a stronger binding energy and this is well captured by the force field employed in our MD simulations. A rescaling of the ethanol dipole moment to $\mu/\mu_0$ = 0.75 and 0.5 reduces the total binding energy for the second type of hydrogen bonding from -4.2 kcal/mol to -2.7 kcal/mol and -1.4 kcal/mol, respectively, which enables the exploration of the influence of the nature of an additive across a wide range of polar interactions and relative hydrophilicity/hydrophobicity. Specifically, we have examined as a function of $\mu/\mu_0$ the dependence of micelle dimensions, distribution of additives inside the micelle, and the phase behavior.

The influence of the binding strength between water and additive on $R_g^2$ is also shown in Figure 4. For strong water-additive binding, *i.e.*, $\mu/\mu_0$ =1.0, $R_g^2$ shows a relatively weak dependence on the additive concentration. By scaling the additive dipole moment to 75% of the original (ethanol) value, the initial trend in the micelle structure as a function of additive concentration is similar, but a more hydrophobic additive systematically increases the micelle dimensions, particularly at higher concentrations. For a much weaker water-additive binding ($\mu/\mu_0$ =0.5), $R_g^2$ shows a strong and monotonic increase with increasing additive concentration.

Figure 5 shows that, as the additive dipole moment is decreasing (*i.e.*, $\mu/\mu_0$=0.75 and 0.5), the additive molecules penetrate inside the micelles and become miscible with $PFO^-$ chains, intimating that the role of additive is switched to that of a co-solvent. In this system, the additive is still miscible with water but prefers to interact with the fluorinated tails of $PFO^-$. However, if

the concentration is further increased for the $\mu/\mu_0$=0.5 system, we observe a phase separation between water-rich and additive-rich phases, with $PFO^-$ surfactant molecules partitioning to the interface between the two solution phases.

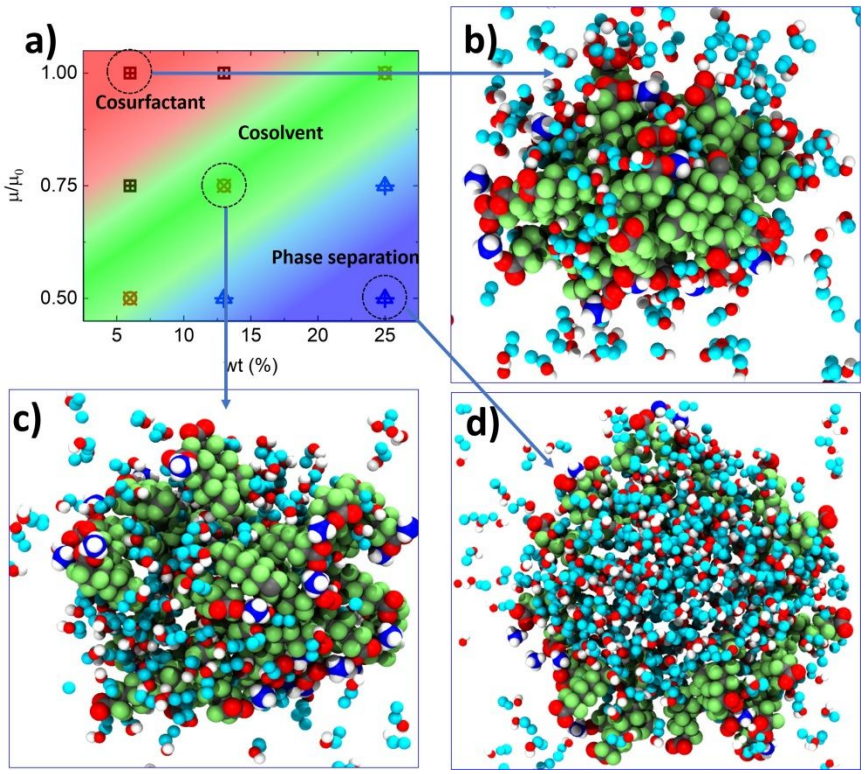


*Figure 6. a) Phase diagram of PFOA/water/additive systems as a function of additive dipole moment and concentration. Panels b), c), and d) show representative structures corresponding to co-surfactant, co-solvent and phase separation regimes, respectively.*

Following a similar analysis for a wide range of concentration/dipole moment combinations, a qualitative phase diagram has been generated and is shown in Figure 6. The co-solvent region can be obtained at lower additive concentrations (compared to what has been observed for ethanol) with more hydrophobic solvents, e.g., additives with $\mu/\mu_0$=0.75 are still in the co-solvent regime at 13 wt% additive concentration, whereas co-solvent behavior is observed at $\mu/\mu_0$=0.75 even at 6 wt% additives. The corresponding micelle morphologies can be found in Figure 6b-d (snapshots for all other systems can be found in Figure S5 of the SI). This indicates

that other potential additives can be used for efficient disruption of PFOA micelles and their removal from water. For instance, the non-toxic diethyl ether might be a promising candidate as it has a molecular dipole moment about 65% that of ethanol and still has reasonable solubility in water.

## Conclusions

The substantial role of ethanol (as a "model" additive) in altering the structure of PFOA micelles in water has been demonstrated by coupling high-resolution experimental measurements with extensive atomistic MD simulations. Both experiments and modeling revealed the formation of well-defined PFOA micelles at concentrations higher than the CMC. Upon the addition of ethanol molecules, the interplay between ethanol and PFOA modulates the PFOA micelle structure. At low ethanol concentrations (less than 13 wt %), a co-surfactant effect of ethanol has been confirmed, whereas a transition to a co-solvent behavior was observed at higher weight fraction of ethanol. In the co-solvent regime, the ethanol molecules penetrate inside the PFOA micelle which correspondingly adopts a more diffuse morphology. MD simulations with scaled dipoles of ethanol showed that the utilization of more hydrophobic (lower dipole moment) additives can shift the co-surfactant to co-solvent behavior transition to even smaller additive concentrations, and hence lead to more efficient disruption of PFOA micelles. Utilization of additives that are too hydrophobic can lead to a phase separation between water-rich and additive-rich phases, with PFOA partitioning to the interface between these phases. The obtained thermodynamic and molecular scale correlations demonstrate that, while there is a complex interplay of several factors defining the micellization of PFOA in solutions, these same factors

can be used to purposely control the PFOA self-assembly with additives and to help design more efficient PFAS removal systems.

## Conflict of interest

The authors declare no competing financial interest.

## Acknowledgements

This research is funded by the U.S. National Science Foundation, grant numbers CBET-1930959 and CBET-1930935. The generous allocation and technical support from the Center for High Performance of Computing at the University of Utah are gratefully acknowledged. We further acknowledge the support of the National Institute of Standards and Technology (NIST), U.S. Department of Commerce, in providing the neutron research facilities used in this work. Access to the CHRNS 30m small-angle neutron scattering instrument was provided by the Center for High Resolution Neutron Scattering (CHRNS), a partnership between the National Institute of Standards and Technology and the National Science Foundation under Agreement No. DMR-1508249. We thank Dr. Yimin Mao at NIST for valuable assistance with the SANS data acquisition. SK acknowledges funding from the Mark Diamond Research Fund (MDRF) of the Graduate Student Association at the University at Buffalo, The State University of New York (SUNY).

## References


1 M. Abe, Synthesis and Applications of Surfactants Containing Fluorine, *Curr. Opin. Colloid Interface Sci.*, 1999, **4**, 354–356.

2 M. P. Krafft, Fluorocarbons and Fluorinated Amphiphiles in Drug Delivery and Biomedical Research, *Adv. Drug Deliv. Rev.*, 2001, **47**, 209–228.

3 K. Wang, G. Karlsson, M. Almgren and T. Asakawa, *J. Phys. Chem. B*, 1999, 103, 9237–9246.

4 K. Matsuoka, E. Takeuchi, M. Takahashi, S. Kitsugi, C. Honda and K. Endo, Solubilization of N-Alkylbenzene and N-Perfluoroalkylbenzene in Hydrogenated and Fluorinated Surfactants Micelles, *J. Colloid Interface Sci.*, 2009, **333**, 641–645.

5 P. McCleaf, S. Englund, A. Östlund, K. Lindegren, K. Wiberg and L. Ahrens, Removal Efficiency of Multiple Poly- and Perfluoroalkyl Substances (PFASs) in Drinking Water Using Granular Activated Carbon (GAC) and Anion Exchange (AE) Column Tests, *Water Res.*, 2017, **120**, 77–87.

6 J. B. N. Mudumbi, S. K. O. Ntwampe, T. Matsha, L. Mekuto and E. F. Itoba-Tombo, Recent Developments in Polyfluoroalkyl Compounds Research: A Focus on Human/Environmental Health Impact, Suggested Substitutes and Removal Strategies, *Environ. Monit. Assess.*, 2017, **189**, 402.

7 A. Blum, S. A. Balan, M. Scheringer, X. Trier, G. Goldenman, I. T. Cousins, M. Diamond, T. Fletcher, C. Higgins, A. E. Lindeman, G. Peaslee, P. de Voogt, Z. Wang and R. Weber, The Madrid Statement on Poly- and Perfluoroalkyl Substances (PFASs), *Environ. Health Perspect.*, 2015, **123**, A107–A111.

8 J. S. Bowman, Response to "Comment on 'Fluorotechnology Is Critical to Modern Life: the Fluorocouncil Counterpoint to The Madrid Statement'", *Environ. Health Perspect.*, 2015, **123**, A170–A171.

9 A. Ritscher, Z. Wang, M. Scheringer, J. M. Boucher, L. Ahrens, U. Berger, S. Bintein, S. K. Bopp, D. Borg, A. M. Buser, I. Cousins, J. Dewitt, T. Fletcher, C. Green, D. Herzke, C. Higgins, J. Huang, H. Hung, T. Knepper, C. S. Lau, E. Leinala, X. Trier, S. Valsecchi, K. van der Jagt and L. Vierke, Zürich Statement on Future Actions on Per- and Polyfluoroalkyl Substances, *Environ. Health Perspect.*, 2018, **126**, 084502.

10 I. T. Cousins, G. Goldenman, D. Herzke, R. Lohmann, M. Miller, C. A. Ng, S. Patton, M. Scheringer, X. Trier, L. Vierke, Z. Wang and J. C. Dewitt, The Concept of Essential Use for Determining When Uses of PFASs Can Be Phased Out, *Environ. Sci. Process. Impacts*, 2019, **21**, 1803–1815.

11 S. Fujii, C. Polprasert, S. Tanaka, N. P. H. Lien and Y. Qiu, New POPs in the Water Environment: Distribution, Bioaccumulation And Treatment of Perfluorinated Compounds - A Review Paper, *J. Water Supply Res. Technol. - AQUA*, 2007, **56**, 313–326.

12 https://www.epa.gov/ground-water-and-drinking-water/drinking-water-health-advisories-pfoa-and-pfos.

13 I. Ross, J. McDonough, J. Miles, P. Storch, P. Thelakkat Kochunarayanan, E. Kalve, J. Hurst, S. S. Dasgupta and J. Burdick, A review of Emerging Technologies for Remediation of PFASs, *Remediation*, 2018, **28**, 101–126.

14 L. Xiao, Y. Ling, A. Alsbaiee, C. Li, D. E. Helbling and W. R. Dichtel, β-Cyclodextrin Polymer Network Sequesters Perfluorooctanoic Acid at Environmentally Relevant

Concentrations, *J. Am. Chem. Soc.*, 2017, **139**, 7689–7692.
15 A. H. Karoyo and L. D. Wilson, Investigation of the Adsorption Processes of Fluorocarbon and Hydrocarbon Anions at the Solid-Solution Interface of Macromolecular Imprinted Polymer Materials, *J. Phys. Chem. C*, 2016, **120**, 6553–6568.
16 D. Q. Zhang, W. L. Zhang and Y. N. Liang, Adsorption of Perfluoroalkyl and Polyfluoroalkyl Substances (PFASs) From Aqueous Solution - A review, *Sci. Total Environ.*, 2019, **694**, 133606.
17 A. M. Bodratti, B. Sarkar and P. Alexandridis, Adsorption of Poly(ethylene oxide)-Containing Amphiphilic Polymers on Solid-Liquid Interfaces: Fundamentals and Applications, *Adv. Colloid Interface Sci.*, 2017, **244**, 132–163.
18 V. Srinivasan and D. Blankschtein, Prediction of Conformational Characteristics and Micellar Solution Properties of Fluorocarbon Surfactants, *Langmuir*, 2005, **21**, 1647–1660.
19 B. Kunze, J. Kalus, N. Boden and M. S. B. Brandao, Transition from Rod-to Disk-like Micelles in APFO/D2O/NH4Cl systems studied by SANS and SAXS, *Phys. B Condens. Matter*, 1997, **234**–**236**, 351–352.
20 S. D. Junior, C. A. Kuhnen and G. R. Ouriques, Theoretical and Experimental Studies of the Aggregation Number in The Ammonium Perfluorooctanoate/Water Binary Mixture, *J. Mol. Liq.*, 2006, **123**, 110–117.
21 S. S. Berr and R. R. M. Jones, Small-angle Neutron Scattering from Aqueous Solutions of Sodium Perfluorooctanoate above the Critical Micelle Concentration, *J. Phys. Chem.*, 1989, **93**, 2555–2558.
22 G. F. Von Rudorff, T. Watermann and D. Sebastiani, Perfluoroalkane Force Field for Lipid Membrane Environments, *J. Phys. Chem. B*, 2014, **118**, 12531–12540.
23 O. Borodin, G. D. Smith and D. Bedrov, A Quantum Chemistry Based Force Field for Perfluoroalkanes and Poly(tetrafluoroethylene), *J. Phys. Chem. B*, 2002, **106**, 9912–9922.
24 G. He, G. Pan and M. Zhang, Assembling Structures and Dynamics Properties of Perfluorooctane Sulfonate (PFOS) at Water–titanium Oxide Interfaces, *J. Colloid Interface Sci.*, 2013, **405**, 189–194.
25 L. A. M. Pereira, L. F. G. Martins, J. R. Ascenso, P. Morgado, J. P. P. Ramalho and E. J. M. Filipe, Diffusion coefficients of fluorinated surfactants in water: Experimental results and prediction by computer simulation, *J. Chem. Eng. Data*, 2014, **59**, 3151–3159.
26 B. Sarkar, S. Lam and P. Alexandridis, Micellization of Alkyl-Propoxy-Ethoxylate Surfactants in Water-polar Organic Solvent Mixtures, *Langmuir*, 2010, **26**, 10532–10540.
27 S. Kancharla, E. Canales and P. Alexandridis, Perfluorooctanoate in aqueous urea solutions: Micelle formation, structure, and microenvironment, *Int. J. Mol. Sci.*, 2019, **20**, 5761.
28 B. Sarkar, V. Ravi and P. Alexandridis, Micellization of Amphiphilic Block Copolymers in Binary and Ternary Solvent Mixtures, *J. Colloid Interface Sci.*, 2013, **390**, 137–146.
29 Y. Lin and P. Alexandridis, Cosolvent Effects on the Micellization of An Amphiphilic Siloxane Graft Copolymer in Aqueous Solutions, *Langmuir*, 2002, **18**, 4220–4231.
30 G. M. Førland, J. Samseth, M. I. Gjerde, H. Høiland, A. O. Jensen and K. Mortensen, Influence of Alcohol on the Behavior of Sodium Dodecylsulfate Micelles, *J. Colloid Interface Sci.*, 1998, **203**, 328–334.
31 J. G. Méndez-Bermúdez and H. Dominguez, Structural Changes of A Sodium Dodecyl Sulfate (SDS) Micelle Induced by Alcohol Molecules, *J. Mol. Model.*, 2016, **22**, 33.

32 E. Caponetti, D. Chillura Martino, M. A. Floriano and R. Triolo, Localization of n-alcohols and Structural Effects in Aqueous Solutions of Sodium Dodecyl Sulfate, *Langmuir*, 1997, **13**, 3277–3283.

33 A. A. Rafati, H. Gharibi and M. Rezaie-Sameti, Investigation of the Aggregation Number, Degree of Alcohol Attachment and Premicellar Aggregation of Sodium Dodecyl Sulfate in Alcohol-Water Mixtures, *J. Mol. Liq.*, 2004, **111**, 109–116.

34 S. Javadian, H. Gharibi, B. Sohrabi, H. Bijanzadeh, M. A. Safarpour and R. Behjatmanesh-Ardakani, Determination of the Physico-chemical Parameters and Aggregation Number of Surfactant in Micelles in Binary Alcohol-Water Mixtures, *J. Mol. Liq.*, 2008, **137**, 74–79.

35 P. C. Griffiths, N. Hirst, A. Paul, S. M. King, R. K. Heenan and R. Farleyt, Effect of ethanol on the Interaction between Poly(Vinylpyrrolidone) and Sodium Dodecyl Sulfate, *Langmuir*, 2004, **20**, 6904–6913.

36 A. I. Fajalia and M. Tsianou, Charging and Uncharging a Neutral Polymer in Solution: A Small-angle Neutron Scattering Investigation, *J. Phys. Chem. B*, 2014, **118**, 10725–10739.

37 R. Zana, Aqueous Surfactant-alcohol Systems: A Review, *Adv. Colloid Interface Sci.*, 1995, **57**, 1–64.

38 M. Almgren and S. Swarup, Size of Sodium Dodecyl Sulfate Micelles in The Presence of Additives I. Alcohols and Other Polar Compounds, *J. Colloid Interface Sci.*, 1983, **91**, 256–266.

39 B. D. Flockhart, The Critical Micelle Concentration of Sodium Dodecyl Sulfate in Ethanol-Water Mixtures, *J. Colloid Sci.*, 1957, **12**, 557–565.

40 K. Yoda, K. Tamori, K. Esumi and K. Meguro, Solubilization of alcohols in single and mixed surfactant aqueous solutions containing fluorocarbon surfactant, *Colloids and Surfaces*, 1991, **58**, 87–98.

41 S. . Milioto and R. De Lisi, Enthalpies of Mixing of Some Primary Hydrogenated and Fluorinated Alcohols and Sodium Perfluorooctanoate Aqueous Solutions, *Langmuir*, 1994, **10**, 1377–1386.

42 C. Treiner and A. K. Chattopadhyay, The Partition Coefficient of Various Alcohols between Water and Alkaliperfluorooctanoate Micelles, *J. Colloid Interface Sci.*, 1984, **98**, 447–458.

43 J. Carlfors and P. Stilbs, Solubilization in sodium perfluorooctanoate micelles: A multicomponent self-diffusion study, *J. Colloid Interface Sci.*, 1985, **103**, 332–336.

44 P. C. Shanks; and E. I. Franses, Estimation of Micellization Parameters of Aqueous Sodium Dodecyl Sulfate from Conductivity Data, 1992, **96**, 1794–1805.

45 H. Xing, P. Yan and J. Xiao, Unusual Location of The Pyrene Probe Solubilized In The Micellar Solutions Of Tetraalkylammonium Perfluorooctanoates, *Soft Matter*, 2013, **9**, 1164–1171.

46 T. Nivaggioli, P. Alexandridis, T. A. Hatton, A. Yekta and M. A. Winnik, Fluorescence Probe Studies of Pluronic Copolymer Solutions as a Function of Temperature, 1995, **11**, 730–737.

47 J. C. Peng; and W. X. J.-X. Chen;, Effect of Counterions on Fluorinated Surfactants 1 . Surface Activity and Micellization, *Acta Chim. Sin.*, 2005, **63**, 279–283.

48 A. J. Prosser and E. I. Franses, Adsorption and Surface Tension of Ionic Surfactants at the Air-water Interface : Review And Evaluation Of Equilibrium Models, *Colloids Surfaces A Physicochem. Eng. Asp.*, 2001, **178**, 1–40.

49 A. Ito;, H. Sakai;, Y. Kondo;, N. Yoshino; and A. Masahiko;, Micellar Solution Properties of Fluorocarbon-Hydrocarbon Hybrid Surfactants, *Langmuir*, 1996, **12**, 5768–5772.

50 S. R. Kline, Reduction and analysis of SANS and USANS data using IGOR Pro, *J. Appl. Crystallogr.*, 2006, **39**, 895–900.

51 P. Taylor, J. B. Hayter and J. Penfold, An analytic structure factor for macroion solutions, *Mol. Phys.*, 1981, **42**, 109–118.

52 H. Iijima, T. Kato, H. Yoshida and M. Imai, Small-angle X-ray and Neutron Scattering from Dilute Solutions of Cesium Perfluorooctanoate. Micellar Growth along Two Dimensions, *J. Phys. Chem. B*, 1998, **102**, 990–995.

53 E. Caponetti, D. C. Martino, M. A. Floriano and R. Triolo, Fluorinated, Protonated, and Mixed Surfactant Solutions: A Small-Angle Neutron Scattering Study, *Langmuir*, 1993, **9**, 1193–1200.

54 A. Downer, J. Eastoe, A. R. Pitt, J. Penfold and R. K. Heenan, Adsorption and Micellisation of Partially- and Fully-fluorinated Surfactants, *Colloids Surfaces A Physicochem. Eng. Asp.*, 1999, **156**, 33–48.

55 D. Bedrov, J.-P. Piquemal, O. Borodin, A. D. MacKerell, B. Roux and C. Schröder, Molecular Dynamics Simulations of Ionic Liquids and Electrolytes Using Polarizable Force Fields, *Chem. Rev.*, 2019, **119**, 7940–7995.

56 O. Borodin, Polarizable Force Field Development and Molecular Dynamics Simulations of Ionic Liquids, *J. Phys. Chem. B*, 2009, **113**, 11463–11478.

57 Y. Kassir, M. Kupiec, A. Shalom and G. Simchen, Canonical dynamics: Equilibrium phase-space distributions, *Curr. Genet.*, 1985, **31**, 1695.

58 I. C. Yeh and M. L. Berkowitz, Ewald Summation for Systems with Slab Geometry, *J. Chem. Phys.*, 1999, **111**, 3155–3162.

59 B. J. Palmer, *J. Comput. Phys.*, 1993, 104, 470–472.

60 Y. Muto, K. Esumi, K. Meguro and R. Zana, Aggregation Behavior of Mixed Fluorocarbon and Hydrocarbon Surfactants in Aqueous Solutions, *J. Colloid Interface Sci.*, 1987, **120**, 162–171.

61 Y. Muto, K. Esumi, K. Meguro and R. Zana, Pyrene Fluorescence as a Probe of Fluorocarbon Micelles and Their Mixed Micelles with Hydrocarbon Surfactants, *Langmuir*, 1988, **4**, 942–945.